Rapid bedrock canyon incision during a mid-Holocene pluvial period, Qilian Shan, China

Yiran Wang[1], Michael E. Oskin[1], Youli Li[2], Huiping Zhang[3]

[1] Department of Earth and Planetary Sciences, University of California, Davis, California, USA

[2] College of Urban and Environmental Sciences, Peking University, Beijing, China

[3] Institute of Geology, China Earthquake Administration, Beijing, China

Corresponding author: Yiran Wang (yrwwang@ucdavis.edu).

Key Points:

- ~ 90 m river incision and ~ 10 km knickzone migration since mid-Holocene.
- Numerical modeling shows the maximum duration of knickzone formation should be about 600yr, which discharge is at least 1.7 times the present.
- Channel width played an important role in knickzone formation.

Abstract

Located at the transition between monsoon and westerly dominated climate systems, major rivers draining the western Qilian Shan incise deep, narrow canyons into latest Quaternary foreland basin sediments of the Hexi Corridor. Field surveys show that the Beida River incised 135 m at mountain front over the Late Pleistocene and Holocene at an average rate of 0.006 m/yr. A steep knickzone, with 3% slope, initiated at the mountain front and has since retreated 10km upstream. Terrace dating results suggest that this knickzone formed around the mid-Holocene, over a duration of less than 1.5 kyr, during which incision accelerated to at least 0.035 m/yr. These incision rates are much larger than the uplift rate across the North Qilian fault, which suggests a climate-related increase in discharge drove rapid incision over the Holocene and formation of the knickzone. Using the relationship between incision rates and the amount of base level drop, we build a bedrock and foreland incision model for the Beida River system. We find that narrowing of channel width plays a key role, as important as increased channel slope, in enhancing the rate of river incision. Our model places the maximum duration of knickzone formation to about 600yr, and the minimum river discharge needed to trigger knickzone formation to be 1.7 times of the present discharge. This period of increased river discharge corresponds to a pluvial lake-filling event at the terminus of the Beida River and correlates with a wet period driven by strengthening of the Southeast Asian Monsoon.

1 Introduction

An incising river responds to tectonic or climatic perturbation by adjusting its slope, expressed by formation of knickpoints or knickzones (Tucker and Whipple, 2002; Crosby and Whipple, 2006; Whittaker, 2012), and through changes of its channel width (Finnegan et al., 2005). Understanding the evolution and migration of knickzones, channel width, and the coupling between these adjustments, is important in unravelling the type, duration, and amplitude of a perturbation (Bishop et al., 2005; Berlin and Anderson, 2007; Attal et al., 2011). Previous studies on headward migrating knickpoints focus on the role of tectonic uplift or a base level fall, and usually regard climate conditions and channel width as constant (eg. Tucker and Whipple, 2002; Crosby and Whipple, 2006; Haviv et al., 2006; Wobus et al., 2006a). Here we present a case of steep, quickly retreating knickzones within the western Qilian Shan, formed under the combined influence of climatic change and lithologic control. Through modeling of incision of the Beida River, as recorded by its profile and stream terraces preserved along its course, we show that a short, but extreme pluvial period, 4 to 5 kyr ago, was responsible for knickzone formation and pronounced narrowing of its channel. The period of rapid bedrock canyon incision corresponds with a high stand of Juyanze paleolake, terminus of the Beida River and adjacent rivers draining the western Qilian Shan (Figure 1).

In western China, the Qilian Shan is the source of several northeast flowing rivers with deep canyons incised across the mountain-basin boundary (Figure 1). As one of these deeply incised rivers, the Beida River is characterized by a prominent knickzone which separates its profile into 3 patches (upper, knickzone, and lower patch; Figure 2). Each patch can be distinguished by different channel slopes and channel widths: gentle and wide upper patch, steep and narrow knickzone, and a lower patch with a gentle slope similar to the upper patch, but a narrower channel. The successive generation and retreat of these patches corresponds to different boundary conditions, and together read as a tape recorder of the incision history at the mountain front.

2 Geological background

The Qilian Shan form the northeastern margin and the youngest growing portion of the Tibetan plateau (Tapponnier et al., 2001). The Hexi Corridor, north of the Qilian Shan, consists of a chain of foreland basins. Bordering arid central Asia, Qilian Shan and Hexi Corridor are occupying the transaction zone between Southeast Asian Monsoon and westerlies (Wei and Gasse, 1999; An et al., 2001). The monsoon brings summer rain in land while the mid-altitude westerlies brings dry air and a small amount of water vapor in winter. The monsoon winds diminish westward as the annual precipitation within the Hexi Corridor decreases from 300~400 mm in the east to <100 mm in the west (Meng et al., 2012). At high altitude within the Qilian Shan (> 4000 m), the precipitation is significantly greater, with an overall trend that also decreases presently from east (>700 mm) to west (~300 mm) (Shi et al., 2006). The modern glacial equilibrium line altitude of Qilian Shan increases from 4400 to 5000 m from northeast to southwest (Shi, 2011), reflecting the decrease in precipitation. Between the year 2005 to 2010, within the Qilian Shan there were 2684 glaciers with a total area of 1597.81 km^2 and an ice volume of 84.48 km^3 (Guo et al., 2014; Sun et al., 2015). These glaciers covered approximately 4% of the landscape above 4000 m elevation. The extent of these glaciers has fluctuated repeatedly throughout the Quaternary. Dating of moraines suggests that glacial advances have occurred during the little ice age (~1300-1850 A.D.), MIS (Marine Isotope Stage) 2, MIS 4, MIS 6, and MIS 12; some glacial expansion may have occurred during MIS 3 as well (Shi et al., 2006).

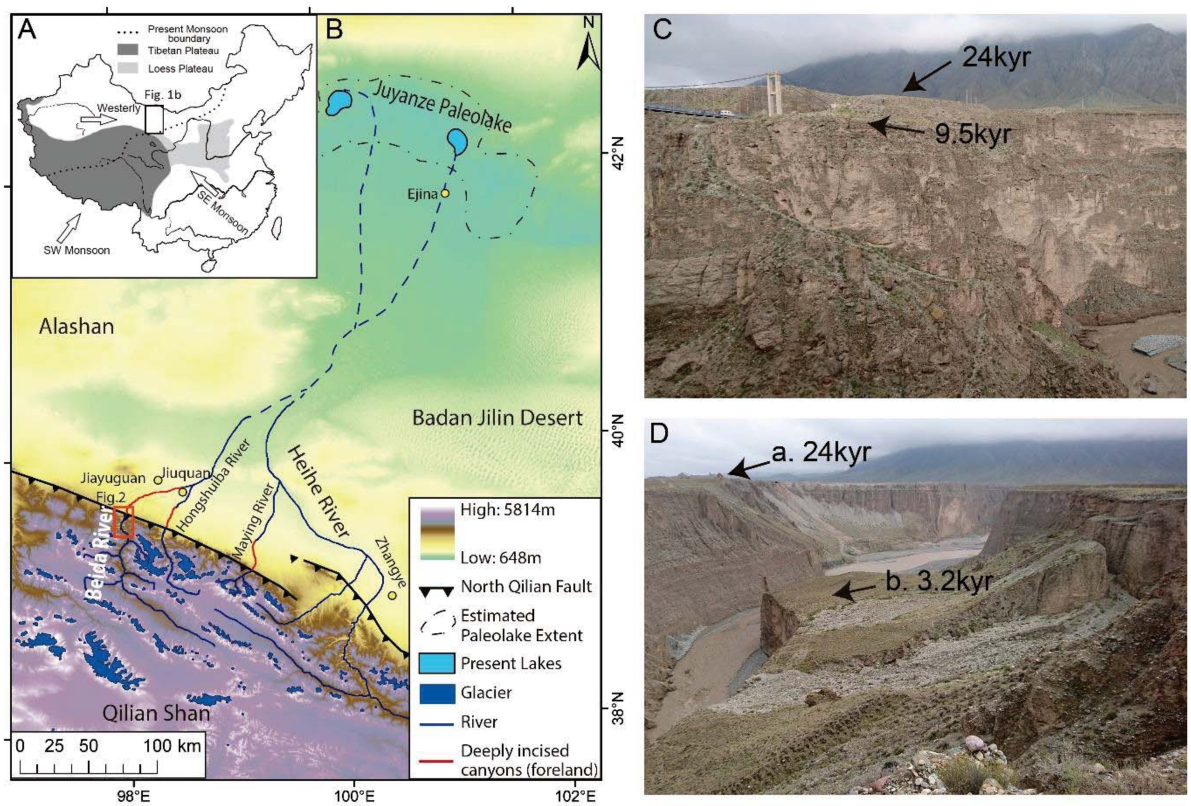

Figure 1 A. Location of our research area with respect to Monsoon and Westerly prevalling area. B. Digital elevation map of the research area and the Heihe Drainage system. Inset photo shows the deeply incised canyon of Beida River at Qilian Shan mountian front. Glacial coverage is mapped based on Raup, B.H (2007). C. Photo of Beida River caynon at mountain front. D. Photo of Beida River canyon in the foreland, with sample site a and b annotated.

The Hei He (river) forms the largest drainage basin in the north Qilian Shan, and terminates within the Juyanze paleolake basin, north of the Hexi Corridor. Three major tributaries, Beida, Hongshuiba, and Maying, join the Hei He from the south and west (Figure. 1). As the largest tributary of Hei He drainage, Beida River is ~360 km long, occupying 6880 km^2 drainage area (Jiuquan History Compilation Committee, 1998). Sediment and core records from the Juyanze paleolake basin indicate frequent dry-wet oscillations over the past 11,000 yr, including highstands during 10700 - 8900 yr BP, 5400 - 4000 yr BP, 2900 - 2700 yr BP, and 2400 - 1500yr BP; and lowstands during 8900 - 8100 yr BP, 7600 - 5400 yr BP, 3200 - 2900 yr BP, and 2600 - 2400 (Mischke et al., 2002, 2005; Herzschuh et al., 2005; Hartmann and Wünnemann, 2009). The highest lake level occurred during the early-Holocene (~20 m deep), and the highest mid-Holocene lake level (~15–17 m deep) occurred at about 4200 yr BP (East Juyanze lake, Hartmann and Wünnemann, 2009).

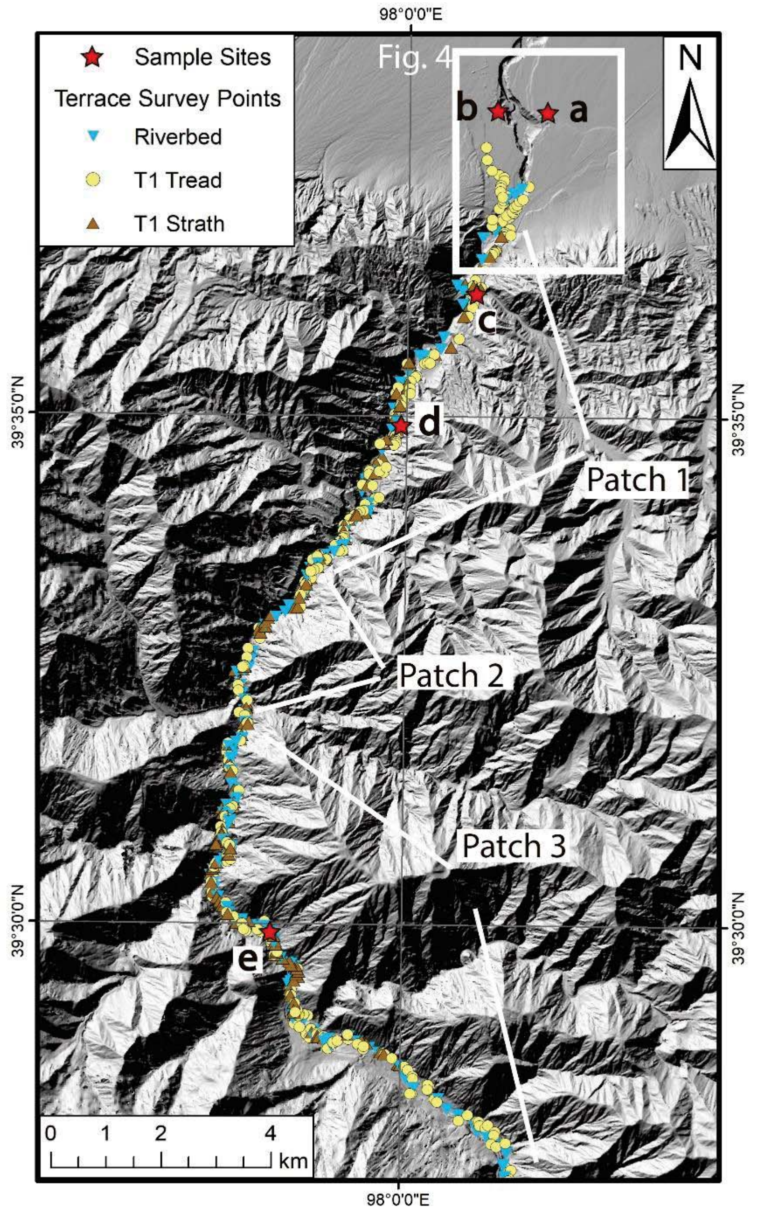

Figure 2 Map of the bedrock Beida River with survey points and geochronology sample sites indicated.

3 Methods

3.1 Field survey

A late Pleistocene fill terrace, up to 60 m thick, is preserved continuously along the narrow, lower bedrock gorge of the Beida River. This terrace grades to an extensive alluvial fan deposit emanating from the mountain front, with minor disruption from reverse fault offsets. The Beida river gorge cuts across the fault-controlled basin boundary, forming a narrow slot canyon up to 135 m deep within the foreland-basin fan gravels. We mapped and surveyed the terrace sequence and the course of Beida River using a laser rangefinder (~0.3 m distance accuracy, 0.25^o inclination accuracy) and differential GPS. Wherever possible, the terrace tread (top of the fluvial gravel), terrace strath (base of fluvial gravel), and present riverbed were measured together (Figure 2). Channel widths were measured from Google Earth imagery at 100 m intervals along the river course. An 8 m resolution digital elevation model, produced by the Polar Geospatial Center (Shean, 2017), augments our field survey data near the mountain front and was used to estimate fault displacements.

3.2 Geochronology

The abandonment age of the Late Pleistocene fill terrace is dated to be 24±3 kyr by combining optically stimulated luminescence (OSL) and Terrestrial Cosmogenic Nuclide (10Be) exposure ages (Figure 2 sample site a; Wang et al., 2019). To document the post-24 kyr incision history of Beida River, we collected charcoal samples from the fine sand and silty overbank deposits on three inset terraces (Figure 2 sample site c, d, e). These overbank deposits were deposited after terrace emplacement, but before incision was sufficient to isolate the terrace surface from flood events. An OSL sample (Figure 2 sample site b) was collected on an even lower insect terrace in the foreland basin from the bottom of the loess covering terrace deposits. Ten charcoal samples were measured at the Keck Carbon Cycle AMS Facility at UC Irvine. The results were calibrated with IntCal14 calibration curve (Reimer et al., 2013) (Table 1). OSL sample (BD-O-12) was processed and measured at the State Key Laboratory of Earthquake Dynamics, China Earthquake Administration. The equivalent doses (De) for the pure fine-grained quartz were determined by the simplified multiple aliquot regenerative-dose (SMAR) protocol (Table 2).

3.3 Bedrock incision

We apply the concept of slope patches (Royden and Perron, 2013) to model the evolution of the Beida River stream profile. The formation of a slope patch is based on stream power, which has the form

$$\frac{dz}{dt} = K\left(\frac{QS}{W}\right)^n \quad , \qquad (1)$$

where z is the channel elevation, t is time, Q is river discharge, S is channel slope, W is channel width, and K and n are an empirical erosional efficiency and exponent, respectively (Whipple and Tucker, 1999; Tucker and Whipple, 2002). To account for downstream increase in discharge, Royden and Perron (2013) transform Q into the variable χ. However, for the case of the Beida River, no major tributary enters along its lower 30 km long course, and thus no transformation is necessary.

A slope patch forms at the channel outlet, with channel slope that develops in balance with the rate of base-level fall. Setting $\frac{dz}{dt}$ to the incision rate, I, at the mountain front, we rearrange equation 1 to solve for this channel slope:

$$S = \left|\frac{dz}{dx}\right| = \left(\frac{I}{K}\right)^{\frac{1}{n}}\left(\frac{W}{Q}\right) \qquad (2)$$

During formation of a slope patch, river profile elevation is found by integrating equation 2 over its finite span x_b to x, assuming constant Q along the channel course:

$$z(x) = \left(\frac{I}{K}\right)^{\frac{1}{n}}\left(\frac{W}{Q}\right)(x - x_b) + z_b = S(x - x_b) + z_b \qquad (3)$$

where x_b and z_b are the horizontal position and elevation of the channel outlet, respectively.

We model the bedrock incision history of the Beida river as a consequence of varying discharge over time that drove incision of its foreland basin deposits. Each slope patch along its course corresponds to a past discharge condition. Once formed, a slope patch retains its gradient as it retreats upstream (Perron and Royden, 2013). The elevation of the (n-1)th slope patch (the patch formed one stage before present) may thus be cast as a function of its slope during formation, $S_{(n-1)}$ and an effective base-level elevation $z_{b(n-1)}$ of the slope patch projected to the outlet position. This base level is predicted by correcting the present base level elevation, z_b, by the difference in the amount of incision across neighboring patches n and n-1,

$$z_{b(n-1)} = z_b + \left(I_{n,n} - I_{n-1,n}\right)t_n. \qquad (4)$$

$I_{n,n}$ is the incision rate of patch n, currently being formed during time interval t_n, directly upstream of the outlet. $_{In-1,n}$ is the incision rate of patch n-1 during that time interval t_n. Note that because discharge has changed, the latter incision rate is different than the incision rate during formation of patch n-1 (i.e. faster for an increase in discharge). For the (n-2)th patch, the effective base level contains two correction terms,

$$z_{b(n-2)} = z_b + \left(I_{n,n} - I_{n-2,n}\right)t_n + \left(I_{n-1,n-1} - I_{n-2,n-1}\right)t_{n-1}. \qquad (5)$$

This may be generalized to additional slope patches, each corrected by the incision rate differences between patches. We apply equations 4 and 5, combined with the incision recorded in stream terraces adjacent to the Beida river, to constrain its discharge history.

3.4 Foreland Basin Incision

The capability of river eroding into the alluvial fan deposits of the foreland is determined by excess sediment transport capacity, resulting in an increase in downstream sediment flux:

$$\frac{dz}{dt} = \frac{1}{\gamma_s}\frac{dq_s}{dx}, \qquad (6)$$

where γ_s is the bulk weight per unit volume of sediment, q_s is sediment discharge per unit channel width(Willgoose et al., 1991; Tucker and Bras, 1998). Unlike bedrock incision, for which information is preserved in channel slope and terrace elevations, we do not possess direct constraints on excess transport capacity and transport efficiency. Nonetheless we can use the diffusive nature of foreland-basin incision as an additional constraint, so long as there exists a linear relationship between discharge and excess sediment transport capacity of the Beida River as it exits the Qilian Shan. Given a linear relationship between unit stream power, QS/W, and q_s (Meyer-Peter and Müller, 1948), predicted incision of the foreland basin is diffusive in character, forming a canyon that both deepens and lengthens downstream of the mountain front over time.

Summed over a time period, Δt, the amount of incision at the mountain front, Δz, is controlled by the excess unit transport capacity of the stream, $[Q_c - Q_s]/W$, as it enters the foreland basin, divided by a diffusion length scale, $\sqrt{\frac{\pi}{4}K_t\frac{Q}{W\Delta t}}$, where constant K_t is the transport efficiency, Q is water discharge, W is channel width, Q_c is the sediment transport capacity, and Q_s is the sediment flux (Humphery & Konard, 2000). No incision occurs when $Q_s = Q_c$. The average gravel incision rate at the mountain front can thus be described by equation:

$$I = \frac{Q_c - Q_s}{W\gamma_s^{1/2}} \left[\frac{\pi}{4} K_t \frac{Q}{W} \Delta t\right]^{-\frac{1}{2}}. \qquad (7)$$

4 Beida River profile and incision history

Presently, the 30 km reach of Beida River upstream of the mountain front is entirely contained within a bedrock channel. Channel slopes, measured directly from fitting the long profile, show a knickzone between 10 to 12 km upstream of the mountain front. The knickzone divides the river profile into three patches: patch 1, upstream of the knickzone, with slope of 0.013; patch 2, the knickzone itself, with slope of 0.029; patch 3, below the knickzone with slope of 0.012. River width also varies, from widest at patch 1 (10 m to 140 m, median 35 m), narrowest within patch (8 m and 29 m, median 17 m) and less narrow along patch 3 (14 m to 70 m, median 26 m).

Table 1 ^{14}C age of Beida River terraces

Sample site	**Sample name**	**Depth (cm)**	**Fraction Modern**	**±**	**$D^{14}C$ (‰)**	**±**	**^{14}C age (yr BP)**	**±**	**Calibarated age**	
									1σ (BP)	**2σ (BP)**
c	BDC-5	23	0.3378	0.0008	-662.2	0.8	8720	20	9611-9699	9561-9737
	BDC-3	28	0.3462	0.0028	-653.8	2.8	8520	70	9473-9544	9332-9340 9404-9632 9645-9657
	BDC-4	32	0.3393	0.0008	-660.7	0.8	8680	20	9557-9630 9647-9653	9552-9679
	BDC-6	45	0.332	0.0009	-668	0.9	8855	25	9895-9949 9990-10012 10025-10038 10061-10134	9784-9848 9861-9878 9883-9966 9982-10155
d	BDC-9	15	0.5715	0.0011	-428.5	1.1	4495	20	5054-5077 5105-5136 5163-5189 5213-5228 5231-5251 5257-5281	5047-5147 5153-5202 5210-5288
	BDC-8	22	0.5973	0.0011	-402.7	1.1	4140	15	4617-4652 4669-4703 4757-4765 4784-4809	4580-4726 4752-4770 4780-4815
	BDC-10	29	0.5862	0.0011	-413.8	1.1	4290	15	4844-4856	4839-4862
e	BDC-14	31	0.4725	0.001	-527.5	1	6025	20	6800-6815 6845-6901	6797-6934

	BDC-11	32	0.4702	0.0012	-529.8	1.2	6060	20	6893-6944	6807-6811 6856-6979
	BDC-12	46	0.4497	0.0029	-550.3	2.9	6420	60	7309-7419	7185-7186 7246-7439

Table 2 OSL age of loess covering terrace tread

Sample Site	Sample no.	U /ppm	Th /ppm	K (%)	Water Content (%)	Dose Rate (Gy/ka)	Equivalent Dose [1] (Gy)	Age [2] (ka)
b	BD-O-12	2.34±0.10	9.32±0.28	1.67±0.06	0	3.5±0.3	11.4±0.7	3.2±0.2

1. Equivalent dose measured using X-ray fluorescence.
2. Uncertainties in equivalent dose, dose rate and age determinations are expressed at the 1σ confidence level.

North of the mountain front, the youngest fill terrace, T1, merges into the extensive 23 kyr alluvial fan. Within the range, the T1 fill deposit ranges from 40 to 80 m of thickness, and consists of unconsolidated medium to poorly sorted, well-rounded boulder-cobble conglomerate and sandy conglomerate. The lithology of the sediments mainly consists of quartzite, granite, slate, and limestone. T1 treads are very well preserved, only covered by 1~2 m loess cap except at tributary junctions, where alluvial fans are deposited upon the tread. The T1 tread presently lies ~130 m above present riverbed of patch 3, and ~60 m above riverbed of patch 1. Bedrock below the T1 strath is exposed continuously for 30 km upstream of the mountain front.

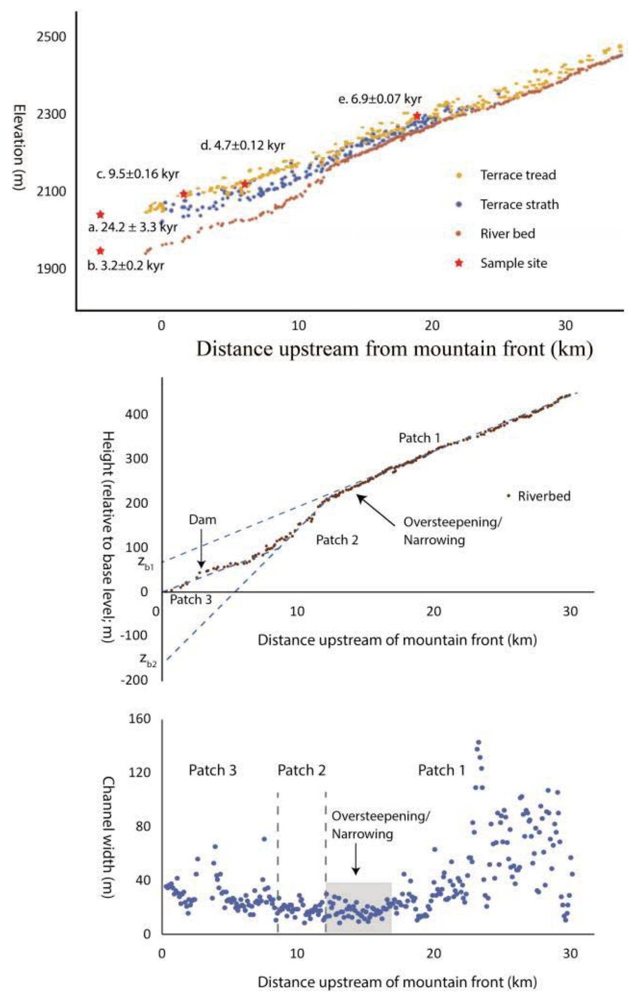

Figure 3 a) Longitudinal profile of the Beida River channel, terrace treads and strath elevations, with sample sites and ages indicated. b) Three patches of Beida river profile, projected to effective base level at the mountain front. c) Channel width measured at 100m intervals along the course of the Beida River.

The most prominent inset terrace, T1', is preserved continuously at an elevation 10 to 15 m lower than T1 tread. ^{14}C dating of charcoal samples at site c (Figure 2, 3a) indicates abandonment of T1' prior to 9.50 ± 0.16 kyr BP. Inset terraces below T1' record progressive incision of the Beida River. An inset terrace at site e, situated 42 m above the present riverbed of patch 1, yielded an age of 6.9 ± 0.07 kyr. At site d, a terrace with tread elevated 90 m above the patch 3 riverbed yielded an age of 4.7 ± 0.12 kyr (Fig.3a, Table 1). 2.5 km downstream of the mountain front in the incised foreland basin deposits, an inset terrace with tread 37 m above the present riverbed yielded an OSL age of 3.2 ± 0.2 kyr from the bottom of the loess covering its tread (Table 2).

The bedrock exposed by incision of Beida river consists of Precambrian marble and gneiss, Middle Cambrian slate, quartzite, and limestone, Lower Ordovician slate, and Middle to Upper Silurian slate (Gansu Geological Bureau, 1989). Though intense folding and faulting occurs within the bedrock outcrops along the Beida river, T1 terrace treads overlying these basement structures show no apparent deformation. At the mountain front, the southern strand of North Qilian fault uplifts the T1 terrace tread by 4.6 m. Two additional strands, located 1 km and 2.5 km north of the main fault, uplift T1 terrace by an additional 1.6 m and 8.6 m, respectively (Figure. 4). Post-9.5 kyr river incision across these active faults of up to 115 m greatly exceeds the sum amount of fault throw of 14.8 m.

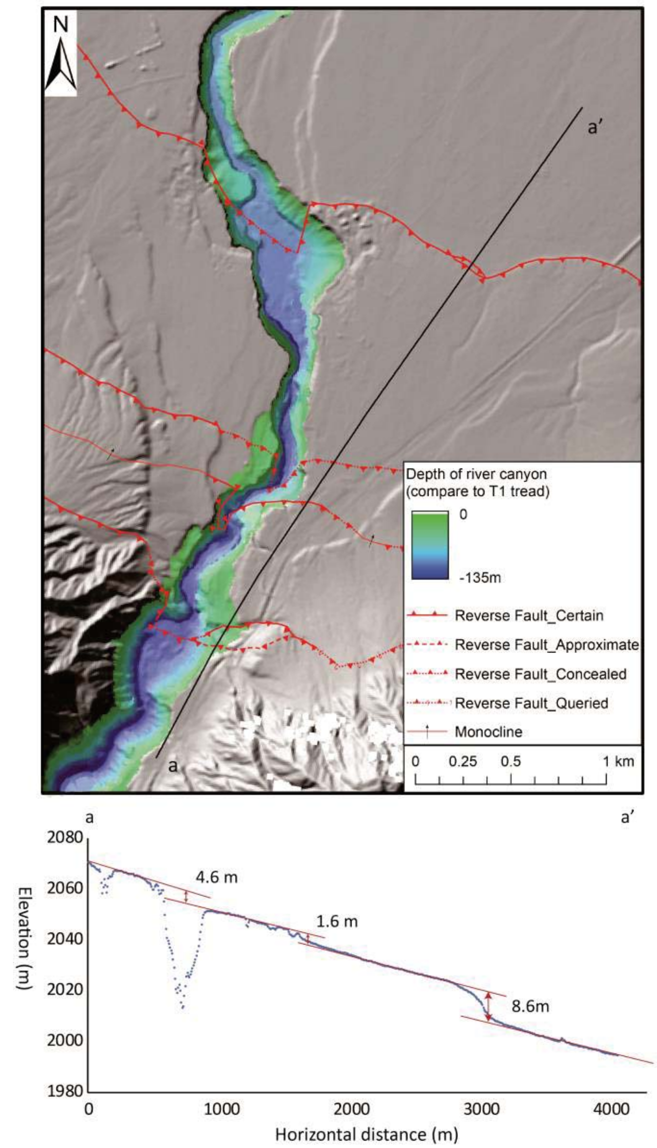

Figure 4 Hillshade map of lower Beida River gorge, colored by channel incision depth below T1 terrace tread. Line a-a' indicates the location of the topographic profile, shown below map, illustrating scarps formed by slip on North Qilian fault zone, extracted from 8m-resolution topography (Shean, 2017).

Based on the terrace ages and height relative to the Beida River, we interpret a three-stage Holocene history of rapid canyon incision near the mountain front. Stage 1 commenced prior to 9.5 kyr BP at a rate of 0.006 ± 0.001 m/yr. This was followed by an acceleration of incision rate to at least 0.035 m/yr during stage 2, commencing sometime after 4.7 ka. At stage 3, starting around 3.2 kyr BP, incision rate slowed again to approximately 0.010 ± 0.002 m/yr.

5 Discussion

5.1 Adjustment of channel slope and width to the change of discharge

We associate the three slope patches along the bedrock channel of the Beida River as formed during the three stages of Holocene incision recorded by its inset terrace record. Each patch initially formed at the mountain front outlet where the bedrock channel transitions to a gravel channel. The formation of each patch was triggered by the changing of the rate of base level fall, resulting from a change in the rate of discharge and incision of foreland-basin deposits. We exclude the possibility of a fixed knickpoint due to lithology control or join of a major tributary, because T1 straths show no signs of knickpoint along the river.

We assume that as each patch forms, channel width is also set and maintained along with the channel slope. We find that the width of Beida River channel narrowed significantly when incision rate increased during formation of patch 2 (Figure 3c), and then remained relatively narrow as incision rate decreased to form patch 3. This suggests that channel width responds both to the incision rate and the inherited prior channel condition. The effect of this inherited channel narrowing is as important as channel slope. For example, the incision rate during formation of patch 3 is roughly twice the incision rate during formation of patch 1 based on terrace records, but the slopes of the two patches are almost the same. The difference in incision rate must be entirely a result of the narrower channel that patch 3 inherited the from patch 2 as this steep knickzone swept upstream.

A 5 km long reach that connects patch 1 and 2 is slightly steeper (0.015 vs 0.013) and much narrower (15m vs. 60m median width) than patch 1 (Figure. 3c). This slightly steepened and narrowed channel is possibly a result of increasing in flow velocity and shear stress immediately above the knickzone (Haviv et al., 2006). We therefore excluded this reach from our analysis.

5.2 Bedrock incision model

The duration of knickzone formation is directly related to the duration of discharge increase. The timing also constrains the value of the stream power exponent, n, necessary to reproduce the retreat of the knickzone upstream. To constrain these, we use known information on the duration and incision rate of patch 3, inferred from the youngest dated terrace along the Beida River (Figure 2, c, site b), together with channel slopes, widths, and effective base levels (Figure 3) measured from the present river channel. From Eq. 4, the effective base level for patch 2 is the

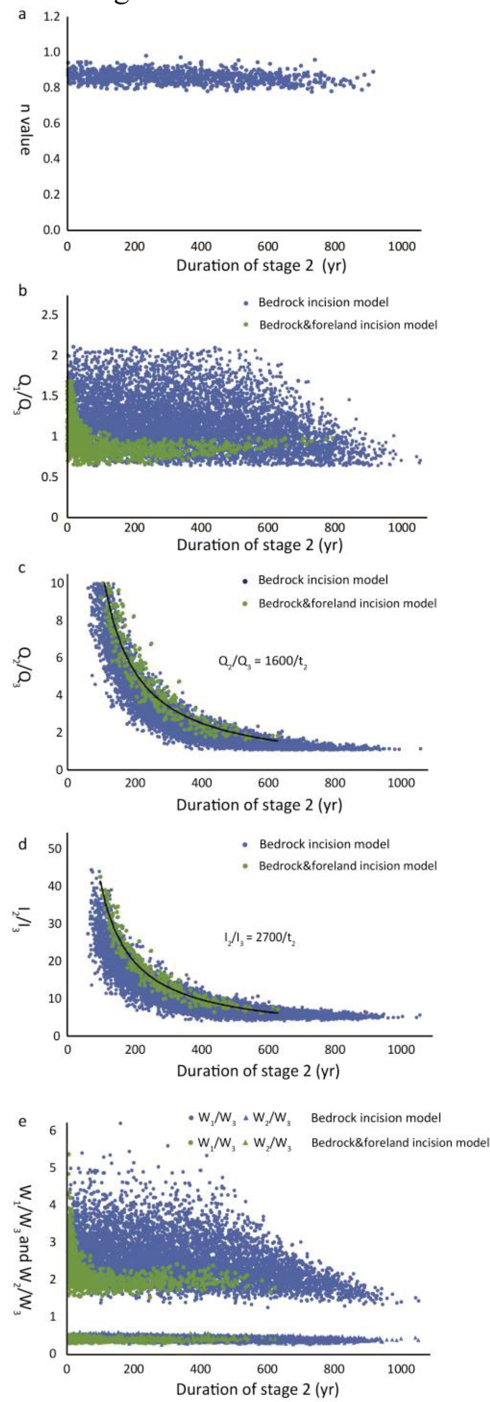

Figure 5 Distributions of Monte Carlo analysis results based on bedrock incision model along (blue) and bedrock and foreland basin combined model (green). a. The distribution of n value related to duration of stage 2. b. The ratios between discharge during stage 1 and present. c. The ratios between discharge during knickzone formation and present. d. The ratios between incision rate during knickzone formation and present. e. The ratios of channel width between different river patches. Data correlated to $Q_2/Q_3 > 10$ are not displayed on figure c and d.

difference incision of patches 2 and 3 during time interval 3:

$$z_{b2} = (I_3 - I_{2,3})t_3 \qquad (8)$$

This equation may be re-arranged to solve for the unknown incision rate of patch 2 during this same interval of time, $I_{2,3} = I_3 - z_{b2}/t_3$. The solution for the stream-power exponent, n, may be calculated from the ratio of incision rates, $I_{2,3}/I_3$.

$$\frac{I_{2,3}}{I_3} = \frac{K\left(\frac{Q_3}{W_2}S_2\right)^n}{K\left(\frac{Q_3}{W_3}S_3\right)^n} = \frac{\left(\frac{S_2}{W_2}\right)^n}{\left(\frac{S_3}{W_3}\right)^n} \qquad (9)$$

$$n = \ln\left(1 - \frac{z_{b2}}{I_3 t_3}\right) / \ln\left(\frac{S_2 W_3}{S_3 W_2}\right) \qquad (10)$$

It is worth noting that because we are considering channel width as spatial variables, the n value doesn't follow the rule with constant channel width where n < 1 means the knickzone would lower its elevation as it migrating upstream.

The duration of knickzone formation and the increase in discharge during this stage can be constrained by finding the difference incision of patch 1 and 2 during the 2nd stage, $(I_2 - I_{1,2})t_2$, with the following relationship:

$$z_{b1} = (I_2 - I_{1,2})t_2 + (I_3 - I_{1,3})t_3. \qquad (11)$$

Equation 11 can be rearranged to

$$(I_2 - I_{1,2})t_2 = [KQ_2^n\left(\frac{S_2}{W_2}\right)^n - KQ_2^n\left(\frac{S_1}{W_1}\right)^n]t_2 = z_{b1} - (I_3 - I_{1,3})t_3 \qquad (12)$$

$$KQ_2^n t_2 = \frac{z_{b1} - (I_3 - I_{1,3})t_3}{\left(\frac{S_2}{W_2}\right)^n - \left(\frac{S_1}{W_1}\right)^n}, \qquad (13)$$

where all variables on the right side of equation 13 are measured, except $I_{1,3}$. The latter may be recast as a function of I_3 via the relationship that $I_{1,3} = K\left(\frac{Q_3}{W_1}S_1\right)^n$ and the ratio, I_3/I_1:

$$\frac{I_3}{I_1} = \frac{K\left(\frac{Q_3}{W_3}S_3\right)^n}{K\left(\frac{Q_1}{W_1}S_1\right)^n} = \left(\frac{Q_3}{Q_1}\right)^n\left(\frac{S_3}{W_3}\right)^n\left(\frac{W_1}{S_1}\right)^n \qquad (14)$$

With some algebraic manipulation, we find:

$$I_{1,3} = \left(\frac{S_1 W_3}{S_3 W_1}\right)^n I_1 \qquad (15)$$

The unknown left-hand side of equation 13 constrains values of both the time, t_2, and discharge, Q_2, during incision of the knickzone. We can explore permissible values for these variables by applying the inequality $I_2 > I_{2,3}$ which states that the incision rate along patch 2 during the formation of the knickzone must be larger than its present incision rate. Therefore, we have

$$KQ_2^n\left(\frac{S_2}{W_2}\right)^n > I_{2,3} \qquad (16)$$

By combining equations 13 and 16, we solve for the maximum duration of t2,

$$t_2 < \frac{z_{b1} - I_3 t_3 + \left(\frac{S_1}{W_1}\right)^n \left(\frac{W_3}{S_3}\right)^n I_1 t_3}{\left[1-\left(\frac{S_1}{W_1}\right)^n \left(\frac{W_2}{S_2}\right)^n\right][I_3 t_3 - z_{b2}]} t_3 \qquad (17)$$

Due to the uncertainty associated with each variable (Table S3), the results may vary largely. In order to have a full picture of the distribution of possible results, we use Monte Carlo analysis to test a range of values for t_2 consistent with the measured values and uncertainty of channel slope, channel width, duration of the latest incision phase t_3, and the projected positions of z_{b1} and z_{b2}. From this we identify populations of paleo-discharge relative to the present, Q_1/Q_3, Q_2/Q_3, and concomitant durations of knickpoint formation.

Because the wide range of uncertainty of each variable, and because equation 17 only constraints the upper limit of t_2, the results of the Monte Carlo analysis may not necessarily fit present channel profile. Therefore, we test each result with two additional constraints on the amount of total incision from our field data. Along patch 3, the Beida river has incised 115 m from T1' tread since 9.5 kyr B.P. Along patch 1, the river has incised 42 m since 6.4 kyr B.P. These incision relationships can be described as:

$$(9.5\text{ka} - t_2 - t_3) \times I_1 + t_2 \times I_2 + t_3 \times I_3 \approx 115m \qquad (18)$$

and

$$(6.4\text{ka} - t_2 - t_3) \times I_1 + t_2 \times I_{1,2} + t_3 \times I_{1,3} \approx 42m \qquad (19)$$

Model results were deemed acceptable if these incision values were met within an error range of ± 5% (Figure 5).

The overall results require a narrow range of n values, between 0.8 to 0.95 (Figure 5a). We find an inverse relationship between the ratio of stage 2 discharge to stage 3 (present) discharge, and the duration of the 2nd stage (Figure 5c). Within 95% confidence, we find permissible discharge for the 2nd stage ranging from slightly elevated (1.04 times present) to extremely elevated (72 times present) with shorter durations requiring larger discharge values (Figure 5d). Modeled durations for stage 2 range between 19 and 830 yr (95% confidence).

5.3 Foreland basin incision model

The above Monte Carlo results are the estimations that only fit bedrock incision model, and do not guarantee that the discharge fluctuation would produce the required base level drop from incision of the foreland basin. The bedrock incision rate immediately upstream of the outlet should be equal to the rate of base level fall resulting foreland basin incision, corrected for tectonic uplift, U:

$$\text{I}_{\text{bedrock}} = \text{I}_{\text{foreland}} - U \qquad (20)$$

Because the uplift rate of the fault strands at mountain front is merely 0.62 m/kyr (14.8 m vertical offset over 24 kyr), much smaller than the lowest erosion rate (6 m/kyr) found in stage 1, therefore may be ignored. Thus, the dominant control on foreland basin incision is excess sediment transport capacity, Q_c-Q_s (Eq. 7). By assuming that both Q_s and Q_c vary linearly with discharge, the excess transport capacity available for channel incision may be expressed as f_sQ - B, where B is a constant background sediment flux and f_s is a discharge-dependent factor.

$$\text{I}_{\text{bedrock}} = \text{I}_{\text{foreland}} = \left(\frac{f_S Q - B}{W {\gamma_s}^{1/2}}\right) \left[\frac{\pi}{4} K_t \frac{Q}{W} \Delta t\right]^{-\frac{1}{2}} \qquad (20b)$$

For this analysis, we assume that foreland channel width did not vary between different incision stages. We justify this assumption from the paucity of inset terraces below T1' tread, suggesting that the river did not narrow significantly as it incised rapidly during stage 2.

For stage 1: $$I_1 = \left(\frac{f_s Q_1 - B}{W\gamma_s{}^{1/2}}\right)\left[\frac{\pi}{4}K_t\frac{Q_1}{W}\Delta t_1\right]^{-\frac{1}{2}} \qquad (21)$$

Stage 2: $$I_2 = \left(\frac{f_s Q_2 - B}{W\gamma_s{}^{1/2}}\right)\left[\frac{\pi}{4}K_t\frac{Q_2}{W}\Delta t_2\right]^{-\frac{1}{2}} \qquad (22)$$

Stage 3: $$I_3 = \left(\frac{f_s Q_3 - B}{W\gamma_s{}^{1/2}}\right)\left[\frac{\pi}{4}K_t\frac{Q_3}{W}\Delta t_3\right]^{-\frac{1}{2}} \qquad (23)$$

Using ratios of equations 21, 22, and 23, the constants fs, γ_s, B, W and Kt may be cancelled out and we find

$$\frac{(Q_3t_3)^{\frac{1}{2}}I_3-(Q_1t_1)^{\frac{1}{2}}I_1}{(Q_2t_2)^{\frac{1}{2}}I_2-(Q_1t_1)^{\frac{1}{2}}I_1}=\frac{Q_3-Q_1}{Q_2-Q_1} \qquad (24)$$

We test families of values of I and Q found from our bedrock incision model with equation 24, retaining solutions if the left-hand side evaluates to within 1% of the value of the right-hand side. These solutions should be compatible with both bedrock and foreland basin incision and can be considered as valid results for Beida River erosion system.

The overall result of the foreland basin model is to narrow the distribution of acceptable model results in relation to the duration of knickzone formation (Figure 5). Acceptable ratios of channel widths, incision rates, and discharge values all fall within narrower bands than constrained from the bedrock channel incision model alone. Under the combined model, longer durations of stage 2 are excluded, but short durations cannot be ruled out. The 95% confidence range for the duration of stage 2 thus condenses to between 2 and 625 yr. The discharge during stage 2 ranges from 1.69 times for the longest duration to over 500 times present for the shortest duration of incision. The minimum incision rate to form the knickzone is 0.070 m/yr.

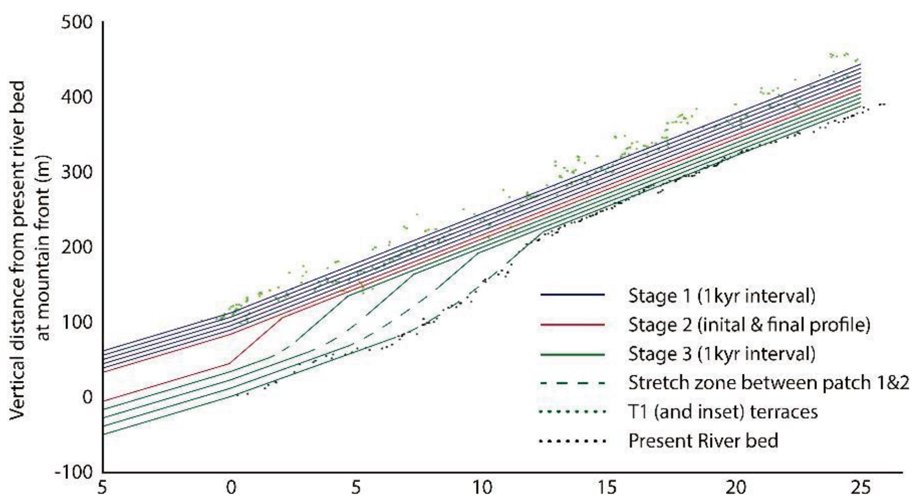

Figure 6 Evolution of river profile simulated using results from our incision model. Field data were also plotted to show the fitness between our model and observation. Variables used in this simulation are: S1=0.0132; S2=0.029; S3=0.012; I1=0.0054m/yr; I2=0.075m/yr; I3=0.011m/yr; T2=533yr.

The relationship between Q_2/Q_3 ratio and duration of stage 2 can be approximated by a simple function: $Q_2/Q_3 \approx 1600/t_2$. In essence, cutting of the steep knickzone of the Beida

River required an excess total discharge, Q_2t_2, equal to about 1600 times the present annual discharge, $Q_3 \times 1\ yr$, spread out over as short as two years or as long as 625 years.

These results could be visualized into channel evolution profiles (Figure 6): a slow incision period of approximately 5 kyr duration since 9.5 kyr followed by a ~600 yr fast incision period which formed a ~40 m high knickzone at mountain front, and then followed by a slow incision period lasted more than 3 kyr till present in which the knickzone migrated upstream for more than 10 km.

5.4 Implications from Beida River knickzone formation

Fluctuations of discharge and the affected incision rates are usually difficult to quantify with river profiles. By constraining incision rates with terraces or other geomorphic features, it is possible to use the amount of base level drop combined with channel slope and width to calculate the amplitude and duration of discharge fluctuation. Our model includes a well constrained bedrock channel incision history, and a less well constrained foreland-basin channel incision record. One of the uncertainties is whether channel width remained constant within the foreland basin. Simulations with varying foreland channel width (Figure 7) show that narrowing of the foreland channel during knickzone formation would predict similar results as the constant channel-width model, though permitting lower threshold discharge and thus a slightly longer maximum duration.

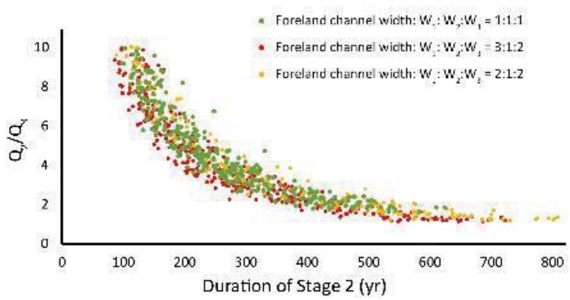

Figure 7 Monte Carlo results with different foreland basin channel width. Green data points: channel width remained constant between different stages. Red data points (group 1): the relative channel width during the 3 stages are 2:1:3. Yellow data points (group 2): the relative channel width during the 3 stages are 2:1:2. Data correlate to Q_2/Q_3 > 10 are not displayed on figure.

Both groups indicate short knickzone formation durations, with the upper boundary for group 1 is 720yr and for group 2 is 800yr (95% confidence). The lower boundaries of Q_2/Q_3 ratios for group 1 is 1.19; for group 2 is 1.24.

In our model, the role of channel width is as important as channel slope and is essential to explain the how the incision rate of patch 3 is significantly higher than patch 1 at a similar channel slope. This reinforces the importance of considering channel width when using a stream power model for bedrock river incision. We find that the power-law exponent, n, falls within a narrow range, between 0.8 and 0.95, from the Beida River incision history (Figure 5a). For a stream power model without considering channel width, n < 1 indicates that the retreating knickpoint should gradually lower its elevation (Royden and Perron, 2013). However, elevation of present Beida River knickpoint is much higher than it originally formed at mountain front (Figure 3), as it has retreated faster than one would predict from its slope alone. This phenomenon can be explained by the narrow channel width, which enhances the incision rate along the knickzone, making it retreat faster, outpacing incision along patch 1.

Overall, our results show how modeling river profile evolution enhances constraints from river terraces along and allows for quantitative bounds on the excess discharge required to produce the observed deep canyon incision. The maximum, and in our view most likely duration of enhanced discharge over a period of ~600 yr is much shorter than the 1.5 kyr duration interpreted from the sparse terrace record. The upper bound on discharge during knickzone formation is difficult to constrain from the channel incision history alone. The most dramatic discharge increase, by a factor of 500, would suggest that the canyon was cut by an outburst flood from a breached lake basin, for which there is no evidence. Also, this would not explain the presence of similar deeply incised canyons on two adjacent large rivers (Maying and Hongshiba, Figure 1). Even a more modest, but still large increase by a factor of 10 would require a large increase in precipitation. This would have dramatically transformed the hydroclimate of the western Qilian Shan and should have led to more widespread effects across the lower elevations of the range than is evident, such as evacuation of hillslope materials and progradation of alluvial fans (e.g., Bull, 1991). Therefore, we favor the longer possible duration, around 600 yr, which would require only a modest increase in precipitation in the western Qilian Shan to level that with present climate in the wetter, central to eastern Qilian Shan.

An alternative source of excess discharge during knickzone formation could have been glacial melt, as has been suggested from the Tian Shan (Malatesta and Avouac, 2018). Such a cause would increase discharge simultaneously for other rivers draining the glaciated highlands of the Qilian Shan, display similar deep canyons and migrating knickpoints (Maying River, Hongshuiba River; Figure 1). However, considering present glacier coverage and discharge from the Beida River shows this explanation to be unlikely. The present ice cover and volume of Beida River drainage are 215.27 km^2 and 8.75 km^3, respectively (Sun et al., 2015). With the present average annual discharge of Beida River, 0.64 km^3 (Ding et al., 1999), a 50% increase of discharge due to excess glacial melt would deplete stored glacial ice in merely 27 yrs. In fact, due to rising temperature, the glacial coverage of Beida River drainage has shrunken at a pace of approximately 9% per decade over the past 50 yrs (Sun et al., 2015), contributing 15% of the average discharge of Beida River. Another study on a glacier west of the Beida River drainage indicates that during Last Glacial Maximum, the paleo-glacier was only 34% larger than the contemporary glacier (Hu et al., 2014). Combining all the evidence, we conclude that the effect of glacial melt cannot be the dominant source of excess discharge needed to trigger knickzone formation.

A multi-century pluvial period punctuated the arid Beida river basin hydroclimate, starting around 4 to 5 kyr B.P., and this pluvial period correlates well with the highest mid-Holocene lake level at 4.2 kyr B.P. recorded by Juyanze Lake records (Hartmann and Wünnemann, 2009). Regionally, evidence for similar humid periods can also be found from Zhuyeze, a lake fed by Shiyang River of Eastern Qilian Shan (Chen, Cheng, et al., 2006), Qinghai Lake (Chen et al., 2016) located within the southeast Qilian Shan, Tianchi Lake of Liupan Shan (AiFeng et al., 2010), and Yanhaizi Lake of Inner Mongolia (Chen et al., 2003). Cave records from upper Hanjiang region and Qinling Mountains (Tan et al., 2018) and stratigraphic sections from Loess Plateau also support the existence of a mid-Holocene humid period (Fang et al., 1999; Fang et al., 2003; Chen et al., 1997; Xiao et al., 2002). In detail, our modeling shows that the pluvial period in the in Beida River drainage was shorter and started a few hundred years later than filling of the Juyanze lake basin. Rapid incision started sometime after 4.7 ± 0.12 kyr B.P., while the high lake level period started earlier, around 5.4 to 5.1 kyr B.P., and lasted a little more than 1 kyr (Mischke et al., 2002, 2005; Hartmann and Wünnemann, 2009). Furthermore, the highest Juyanze lake level, recorded between 10.7 to 8.9 kyr B.P., or the early Holocene optimum (Early Holocene to 7 kyr B.P.) recorded in more easterly paleoclimate archive, is not reflected by the Beida River incision records. In fact, Beida River terrace records indicate that it has the lowest incision rate (thus lowest water discharge) during late Pleistocene and early Holocene. We hypothesize that the brief, singular incision event recorded by the Beida river is a result of its location within the westernmost Qilian Shan. The Qilian Shan and Hexi Corridor occupy the transitional zone between the Southeast Asian monsoon and the westerlies, with wet periods corresponding to increased monsoon influence (Tan et al., 2018). Thus, the mid-Holocene highstand of the Juyanze Lake may have been initiated by increase monsoon influence and discharge from Hei He river draining areas to the east. Therefore, we hypothesize that during early Holocene, the humid Asian monsoon expanded to the central Qilian Shan, where it affected Hei He main stem and filled Juyanze lake to its highest lake level. During the mid-Holocene, the Asian monsoon again expanded to influence Hei He drainage around 5.4 to 5.1 kyr B.P., and then expanded further to the western Qilian Shan and Beida River subdrainage a few hundred years later. In short, between 24 kyr~9.5 kyr B.P., Beida River drainage was under Westerlies' dominant with low incision rate of 1.5 m/kyr, between 9.5~4.7 kyr B.P. Beida River was under weak SE Monsoon influence with an average incision rate of 6 m/kyr; under strong SE Monsoon influence, a pluvial event occurred sometime between 4.7~3.2 kyr B.P. and lasted about 600 yr with a minimum incision rate of 70 m/kyr; after 3.2 kyr B.P., the effect of SE Monsoon weakened and the incision rate dropped back to 10 m/kyr (Figure 8 and 9).

5 Conclusions

The Beida River in the North Qilian Shan has incised deeply into both the bedrock and the adjacent foreland basin sediments. These incision rates greatly exceed rates of tectonic uplift here. Our work demonstrates the capability of bedrock rivers in arid regions to incise deep channels and form fast retreating knickpoints within short period. Field investigation and geomorphic mapping identify a 24 kyr fill terrace, T1, and several sets of inset terraces below. The longitudinal profile of the present river channel preserves a steep knickzone, presently located 10 km upstream of the mountain front. Terrace ages, and relationships between terrace treads and the riverbed, indicate that the knickzone was formed quickly after 4.7kyr BP, driven by an increase of river discharge. By applying the concept of slope patches to bedrock canyon incision, and a diffusive model to foreland-basin incision, we model this Holocene incision history and estimate that river discharge during knickzone formation was at least 1.7 times the present discharge. We further constrain the duration of this period of increased discharge to be less than 600 yr, which is almost 1 kyr shorter than estimated from the sparse terrace age record. Our modeling also reveals how the evolution of channel width plays a crucial role in bedrock erosion process, and that channel narrowing during a period of rapid incision may leave its imprint on later incision stages. The period of increased discharge identified from the Beida River correlates to a pluvial period recorded at the terminal Juyanze lake. The likely cause of rapid incision of the Beida River, and adjacent rivers with similar deeply incised canyons, is the increased influence of the southeast

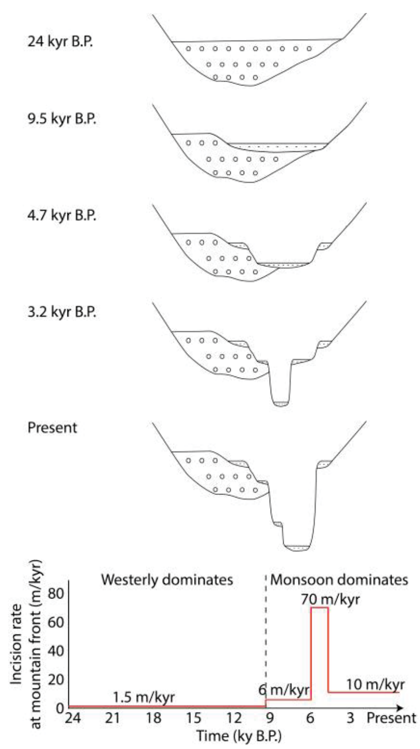

Figure 8 Schematic cross sections (top) of Beida River channel evolution and the diagram of incision rate vs. time (bottom) since 24 kyr B.P.

Asian Monsoon over the Holocene, with the most rapid incision period corresponding to a strengthening of monsoon influence ca. 4.7 kyr B.P.

Acknowledgments, Samples, and Data

This work was supported by the US National Science Foundation [grant number EAR-1524734] to Michael Oskin, the National Natural Science Foundation of China [grant number 41571001] to Youli Li, the Second Tibetan Plateau Scientific Expedition and Research (STEP) [grant number 2019QZKK0704] and the National Natural Science Foundation of China (grant number 41622204; 41761144071) to Huiping Zhang, and through Cordell Durrell Geology Field Fund to Yiran Wang. We are preparing our data for placement in a permanent repository at Dryad (https://datadryad.org/stash). Data that are to be deposited are included as supplementary tables that accompany this manuscript.

References

AiFeng, Z., HuiLing, S., Fahu, C., Yan, Z., ChengBang, A., GuangHui, D., et al. (2010). High-resolution climate change in mid-late Holocene on Tianchi Lake, Liupan Mountain in the Loess Plateau in central China and its significance. Chinese Science Bulletin, 55(20), 2118–2121. https://doi.org/10.1007/s11434-010-3226-0

An, Z., Kutzbach, J. E., Prell, W. L., & Porter, S. C. (2001). Evolution of Asian monsoons and phased uplift of the Himalaya - Tibetan plateau since Late Miocene times. Nature, 411(6833), 62–66. https://doi.org/10.1038/35075035

Attal, M., Cowie, P. A., Whittaker, A. C., Hobley, D., Tucker, G. E., & Roberts, G. P. (2011). Testing fluvial erosion models using the transient response of bedrock rivers to tectonic forcing in the Apennines, Italy. Journal of Geophysical Research: Earth Surface, 116(2), 1–17. https://doi.org/10.1029/2010JF001875

Berlin, M. M., & Anderson, R. S. (2007). Modeling of knickpoint retreat on the Roan Plateau, western Colorado. Journal of Geophysical Research: Earth Surface, 112(3), 1–16. https://doi.org/10.1029/2006JF000553

Bishop, P., Hoey, T. B., Jansen, J. D., & Lexartza Artza, I. (2005). Knickpoint recession rate and catchment area: The case of uplifted rivers in Eastern Scotland. Earth Surface Processes and Landforms, 30(6), 767–778. https://doi.org/10.1002/esp.1191

Bull, W. B. (1991). Geomorphic responses to climatic change. United States.

Chen, C. T. A., Lan, H. C., Lou, J. Y., & Chen, Y. C. (2003). The dry Holocene Megathermal in Inner Mongolia. Palaeogeography, Palaeoclimatology, Palaeoecology, 193(2), 181–200. https://doi.org/10.1016/S0031-0182(03)00225-6

Chen, Fahu, Bloemendal, J., Wang, J. M., Li, J. J., & Oldfield, F. (1997). High-resolution multi-proxy climate records from Chinese Loess: Evidence for rapid climatic changes over the last 75 kyr. Palaeogeography, Palaeoclimatology, Palaeoecology, 130(1–4), 323–335. https://doi.org/10.1016/S0031-0182(96)00149-6

Chen, Fahu, Wu, D., Chen, J., Zhou, A., Yu, J., Shen, J., et al. (2016). Holocene moisture and East Asian summer monsoon evolution in the northeastern Tibetan Plateau recorded by Lake

Qinghai and its environs: A review of conflicting proxies. Quaternary Science Reviews, 154, 111–129. https://doi.org/10.1016/j.quascirev.2016.10.021

Chen, FaHu, Cheng, B., Zhao, Y., Zhu, Y., & Madsen, D. B. (2006). Holocene environmental change inferred from a high-resolution pollen record, Lake Zhuyeze, arid China. Holocene, 16(5), 675–684. https://doi.org/10.1191/0959683606hl951rp

Crosby, B. T., & Whipple, K. X. (2006). Knickpoint initiation and distribution within fluvial networks: 236 waterfalls in the Waipaoa River, North Island, New Zealand. Geomorphology, 82(1–2), 16–38. https://doi.org/10.1016/j.geomorph.2005.08.023

Ding, Y., Ye, B., & Liu, S. (1999). Effect of Climatic Factors on Streamf low in the Alpine Catchmen t of the Qilian Mountains. Acta Geologica Sinica, 54(5), 431–437.

Fang, X., Lü, L., Mason, J. A., Yang, S., An, Z., Li, J., & Zhilong, G. (2003). Pedogenic response to millennial summer monsoon enhancements on the Tibetan Plateau. Quaternary International, 106–107, 79–88. https://doi.org/10.1016/S1040-6182(02)00163-5

Fang, X. M., Ono, Y., Fukusawa, H., Bao-Tian, P., Li, J. J., Dong-Hong, G., et al. (1999). Asian summer monsoon instability during the past 60,000 years: Magnetic susceptibility and pedogenic evidence from the western Chinese Loess Plateau. Earth and Planetary Science Letters, 168(3–4), 219–232. https://doi.org/10.1016/S0012-821X(99)00053-9

Finnegan, N. J., Roe, G., Montgomery, D. R., & Hallet, B. (2005). Controls on the channel width of rivers: Implications for modeling fluvial incision of bedrock. Geology, 33(3), 229–232. https://doi.org/10.1130/G21171.1

Gansu Geological Bureau. (1989). Regional Geology of Gansu Province [in Chinese]. Beijing: Geological Publishing House.

Guo, W., Xu, J., Liu, S., Shangguan, D., Wu, L., Yao, X., et al. (2014). The Second Glacier Inventory Dataset of China (Version 1.0). Cold and Arid Regions Science Data Center at Lanzhou. https://doi.org/10.3972/glacier.001.2013.db

Hartmann, K., & Wünnemann, B. (2009). Hydrological changes and Holocene climate variations in NW China, inferred from lake sediments of Juyanze palaeolake by factor analyses. Quaternary International, 194(1–2), 28–44. https://doi.org/10.1016/j.quaint.2007.06.037

Haviv, I., Enzel, Y., Whipple, K. X., Zilberman, E., Stone, J., Matmon, A., & Fifield, L. K. (2006). Amplified erosion above waterfalls and oversteepened bedrock reaches. Journal of Geophysical Research: Earth Surface, 111(4), 1–11. https://doi.org/10.1029/2006JF000461

Herzschuh, U., Zhang, C., Mischke, S., Herzschuh, R., Mohammadi, F., Mingram, B., et al. (2005). A late Quaternary lake record from the Qilian Mountains (NW China): Evolution of the primary production and the water depth reconstructed from macrofossil, pollen, biomarker, and isotope data. Global and Planetary Change, 46(1-4 SPEC. ISS.), 361–379. https://doi.org/10.1016/j.gloplacha.2004.09.024

Hu, G., Yi, C., Zhang, J., Liu, J., Jiang, T., & Qin, X. (2014). Optically stimulated luminescence dating of a moraine and a terrace in Laohugou valley, western Qilian Shan, northeastern Tibet. Quaternary International, 321, 37–49. https://doi.org/10.1016/j.quaint.2013.12.019

Humphrey, N. F., & Konrad, S. K. (2000). River incision or diversion in response to bedrock uplift. *Geology*, *28*(1), 43–46. https://doi.org/10.1130/0091-7613(2000)028<0043:RIODIR>2.3.CO;2

Jiuquan History Compilation Committee. (1998). Jiuquan City Chorography. Lanzhou: Lanzhou University Press. 108-117.

Malatesta, L. C., & Avouac, J. P. (2018). Contrasting river incision in north and south Tian Shan piedmonts due to variable glacial imprint in mountain valleys. Geology, 46(7), 659–662. https://doi.org/10.1130/G40320.1

Meng, X., Zhang, S., & Zhang, Y. (2012). The Temporal and Spatial Change of Temperature and Precipitation in Hexi Corridor in Recent 57 Years. Acta Geologica Sinica, 67(11), 1482–1492.

Meyer-Peter, E., & Müller, R. (1948). Formulas for bed-load transport. In IAHSR 2nd meeting, Stockholm, appendix 2. IAHR.

Mischke, S., Fuchs, D., Riedel, F., & Schudack, M. E. (2002). Mid to Late Holocene palaeoenvironment of Lake Eastern Juyanze (north-western China) based on ostracods and stable isotopes Paléoenvironnement moyen à tardif du Lac Juyanze d ' Est (NO de la Chine) sur la base des données concernant les ostracodes et. Geobios, 35, 99–110.

Mischke, S., Demske, D., Wünnemann, B., & Schudack, M. E. (2005). Groundwater discharge to a Gobi desert lake during Mid and Late Holocene dry periods. Palaeogeography, Palaeoclimatology, Palaeoecology, 225(1–4), 157–172. https://doi.org/10.1016/j.palaeo.2004.10.022

Raup, B., Racoviteanu, A., Khalsa, S. J. S., Helm, C., Armstrong, R., & Arnaud, Y. (2007). The GLIMS geospatial glacier database: A new tool for studying glacier change. Global and Planetary Change, 56(1–2), 101–110. https://doi.org/10.1016/j.gloplacha.2006.07.018

Reimer, P., Bard, E., Bayliss, A., Beck, J., Blackwell, P., Ramsey, C. B., et al. (2013). IntCal13 and Marine13 Radiocarbon Age Calibration Curves 0–50,000 Years cal BP. Radiocarbon, 55(4), 1869–1887.

Royden, L., & Perron, J. T. (2013). Solutions of the stream power equation and application to the evolution of river longitudinal profiles. Journal of Geophysical Research: Earth Surface, 118(2), 497–518. https://doi.org/10.1002/jgrf.20031

Shean, D. (2017). High Mountain Asia 8-meter DEM Mosaics Derived from Optical Imagery, Version 1, 20170716_tile-224, tile-257, Boulder, Colorado USA. NASA National Snow and Ice Data Center Distributed Active Archive Center. https://doi.org/https://doi.org/10.5067/KXOVQ9L172S2

Shi, Y. (2011). New Understanding of Quaternary Glaciations in China. Shanghai (In Chinese): Shanghai Popular Science Press.

Shi, Y., Cui, Z., & Su, Z. (2006). The Quaternary Glaciations and Environmental Variations in China. Shijiazhuang (In Chinese): Hebei Science and Technology Press.

Sun, M., Liu, S., Yao, X., Guo, W., & Xu, J. (2015). Glacier changes in the Qilian Mountains in the past half century: Based on the revised First and Second Chinese Glacier Inventory. Acta

Geographica Sinica (In Chinese with English Abstract), 70(9), 1402–1414. https://doi.org/10.11821/dlxb201509004

Tan, L., Cai, Y., Cheng, H., Edwards, L. R., Gao, Y., Xu, H., et al. (2018). Centennial- to decadal-scale monsoon precipitation variations in the upper Hanjiang River region, China over the past 6650 years. Earth and Planetary Science Letters, 482, 580–590. https://doi.org/10.1016/j.epsl.2017.11.044

Tapponnier, P., Xu, Z., Roger, F., Meyer, B., Arnaud, N., Wittlinger, G., & Yang, J. (2001). Oblique Stepwise Rise and Growth of the Tibet Plateau. Science, 294(5547), 1671–1677. https://doi.org/10.1126/science.105978

Tucker, G. E., & Whipple, K. X. (2002). Topographic outcomes predicted by stream erosion models: Sensitivity analysis and intermodel comparison. Journal of Geophysical Research: Solid Earth, 107(B9), ETG 1-1-ETG 1-16. https://doi.org/10.1029/2001JB000162

Tucker, G. E., & Bras, R. L. (1998). Hillslope processes, drainage density, and landscape morphology. Water Resources Research, 34(10), 2751–2764. https://doi.org/10.1029/98WR01474

Wang, Y., Oskin, M. E., Zhang, H., Li, Y., Hu, X., & Lei, J. (2019). Deducing Crustal-scale Reverse-Fault Geometry and Slip Distribution from Folded River Terraces, Qilian Shan, China. Tectonics. In press

Wei, K., & Gasse, F. (1999). Oxygen isotopes in lacustrine carbonates of West China revisited: Implications for post glacial changes in summer monsoon circulation. Quaternary Science Reviews, 18(12), 1315–1334. https://doi.org/10.1016/S0277-3791(98)00115-2

Whipple, K. X., & Tucker, G. E. (1999). Dynamics of the stream-power river incision model: Implications for height limits of mountain ranges, landscape response timescales, and research needs. Journal of Geophysical Research, 3(2), 221–222. Retrieved from http://dx.doi.org/10.1029/1999JB900120; doi:10.1029/1999JB900120

Whittaker, A. C. (2012). How do landscapes record tectonics and climate? Lithosphere, 4(2), 160–164. https://doi.org/10.1130/RF.L003.1

Willgoose, G., Bras, R. L., & Rodriguez Iturbe, I. (1991). A coupled channel network growth and hillslope evolution model: 1. Theory. Water Resources Research, 27(7), 1671–1684. https://doi.org/10.1029/91WR00935

Wobus, C., Whipple, K. X., Kirby, E., Snyder, N., Johnson, J., Spyropolou, K., et al. (2006). Tectonics from topography: Procedures, promise, and pitfalls. Special Paper 398: Tectonics, Climate, and Landscape Evolution, 2398(October 2015), 55–74. https://doi.org/10.1130/2006.2398(04)